

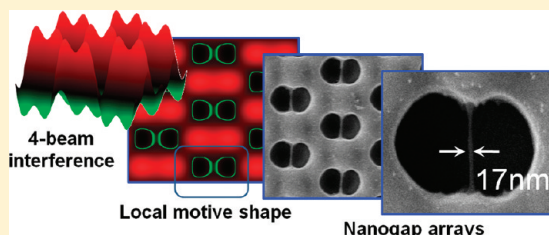
# Holographic Control of Motive Shape in Plasmonic Nanogap Arrays

Xi Zhang, Martin Theuring, Qiang Song, Weidong Mao, Milan Begliarbekov, and Stefan Strauf\*

Department of Physics and Engineering Physics, Stevens Institute of Technology, 1 Castle Point on Hudson, New Jersey, 07030, United States

 Supporting Information

**ABSTRACT:** Here we demonstrate that 4-beam holographic lithography can be utilized to create plasmonic nanogaps that are 70 times smaller than the laser wavelength (488 nm). This was achieved by controlling phase, polarization, and laser beam intensity in order to tune the relative spacing of the two sublattices in the interference pattern of a compound-lattice in combination with the nonlinear resist response. Exemplarily, twin and triplet motive features were designed and patterned into polymer in a single exposure step and then transferred into gold nanogap arrays resulting in an average gap size of 22 nm and smallest features down to 7 nm. These results extend the utility of high-throughput, wafer-scale holographic lithography into the realm of nanoplasmonics.



**KEYWORDS:** Holographic lithography, nanoplasmonics, nanogaps, nanoantenna, compound lattice

Plasmonic nanostructures have recently attracted a great deal of research attention due to their ability to generate surface plasmons that lead to localization of electromagnetic energy well below the diffraction limit.<sup>1,2</sup> Localized surface plasmon resonances (LSPR) can dramatically enhance the light-matter interaction as is evident in surface-enhanced Raman scattering (SERS)<sup>3–5</sup> enabling applications such as ultrasensitive chemical and biological sensing<sup>2,6–10</sup> down to the level of single molecules,<sup>11</sup> monitoring of shape dependent catalysis,<sup>12,13</sup> and miniaturization of photonic circuits.<sup>14,15</sup> Consequently, high-throughput wafer-scale fabrication techniques for metallic nanogap arrays are essential for realizing plasmonic device applications. Previously electron beam lithography,<sup>16–18</sup> focused ion beam milling,<sup>19</sup> and nanocoating<sup>4,5</sup> have been utilized to produce sub-10 nm metallic gaps in order to maximize the effect of LSPR.

Holographic lithography<sup>20</sup> (HL) is an appealing optical technique to create nanopatterns with high throughput over wafer-scale dimensions without the need for electron or ion beams, prefabricated masks, prepatterned wafers, or atomic layer deposition. Two-beam HL was previously utilized to pattern gratings with half pitch as small as 22 nm utilizing excimer lasers and nonlinear processes<sup>21</sup> or index matching fluids<sup>22</sup> in order to reduce feature sizes within the diffraction limit. Extending the geometry to three or more optical beams allows fabrication of complex structures such as photonic crystal lattices<sup>23–27</sup> including all fourteen Bravais lattices,<sup>24</sup> quasi crystals,<sup>28,29</sup> chiral structures,<sup>30</sup> metamaterials,<sup>31</sup> compound lattices,<sup>32,33</sup> and lattices with high-order symmetries.<sup>34</sup> However, the achievable lattice constant of these complex structures is experimentally limited to about 1  $\mu\text{m}$ ,<sup>23–34</sup> and the technique has not yet been applied to the fabrication of metallic nanogap arrays.

In this work we show how to utilize HL for the fabrication of metallic nanogap arrays with sub-10 nm features using a laser wavelength of 488 nm. We show how the gap size can be precisely controlled within the motif shape of a compound lattice

featuring single and double gaps over the nanogap array by proper phase, intensity, and polarization control in a single exposure process. Polymer structures were used as templates to produce the desired metallic nanogap arrays. Consequently, this technique extends the applicability of HL to the realm of nanoplasmonics as well as other applications that require nanoscale patterning such as photonic crystal nanolasers,<sup>35,36</sup> antidot superlattices,<sup>37</sup> and nanofluidic arrays.<sup>38</sup>

**Theoretical Considerations.** In this section, we show how the motive shape in four-beam HL can be systematically optimized to result in features with narrow gap sizes. The intensity profile created by interfering  $N$  linearly polarized laser beams can be described as a sum of the individual sub components as  $I = |\sum_{j=1}^N E_j \exp[i(\vec{k}_j \cdot \vec{r} + \delta_j)]\vec{e}_j|^2$ , where  $E_j$  is the amplitude of the electrical field,  $\vec{k}_j$  is the wave vector,  $\delta_j$  is the initial phase, and  $\vec{e}_j$  is the orientation of the linear polarization vector of the  $j$ th beam. The translational symmetry and lattice constant of the resultant interference patterns can be thus determined by the appropriate choice of the wave vectors,<sup>23</sup> which is experimentally realized by changing the incident angle and position in the projected plane. The angles for the umbrella-like arrangement of the four beams ( $N = 4$ ) shown schematically in Figure 1 were chosen to create a hexagonal lattice featuring a higher density of motives as compared to a simple square lattice. The wave vectors required to generate this pattern are  $\vec{k}_1 = k[-\sin \alpha, 0, \cos \alpha]$ ,  $\vec{k}_2 = k[\sin \alpha, \cos(-\pi/3), \sin \alpha \sin(-\pi/3), \cos \alpha]$ ,  $\vec{k}_3 = k[\sin \alpha \cos(\pi/3), \sin \alpha \sin(\pi/3), \cos \alpha]$ ,  $\vec{k}_4 = k[\sin \alpha, 0, \cos \alpha]$ , where  $\alpha$  is incident angle and  $k = 2\pi/\lambda$ .

In order to control the motive shape and interference contrast one has to vary the parameters  $E_j$ ,  $\delta_j$ , and  $\vec{e}_j$ , i.e. the beam intensity, initial phase and the orientation of the polarization vectors.

**Received:** March 24, 2011

**Revised:** June 9, 2011

**Published:** June 14, 2011

While the variation of these parameters does not change the translational symmetry or the principal lattice constant, it offers the ability to define a compound lattice with local twin or triplet motives at each site of the hexagonal lattice. The compound lattice offers the possibility to tune the relative spacing of features within the local motive shape, i.e. the relative spacing of the two sublattices. This allows defining nanometer-sized gaps that are not limited by the laser wavelength used to write the interference pattern. Thus the introduction of a fourth beam in HL decouples the achievable minimum local feature size in the periodic interference pattern from the achievable lattice constant. The final experimental feature size is a combination of the controlled modifications to the motive shape and the nonlinear response of the photoresist at a particular exposure dose, as further illustrated in the Supporting Information.

In order to systematically study the influence of each of the HL parameters, we first assume that there is no phase difference between the four beams. The orientation of the polarization vectors is described through the angle  $\theta$ , where  $\theta = 0^\circ$  and  $\theta = 90^\circ$  corresponds to p and s polarized states, respectively. The polarization vector of each beam is set to  $0^\circ$ , corresponding to a linear polarization state where each beam lies in the plane spanned by its k-vector and the sample surface normal. As a result, circlelike structures are formed that are arranged in a simple hexagonal lattice, as shown in the contour plots of the three-dimensional (3D) interference patterns in the top left panel of Figure 2a. Furthermore, in order to create a compound lattice a phase delay  $\Delta\delta$  must be introduced into one of the four beams, as shown in the contour plots in Figure 2a, where a phase delay was

added into the second beam. The red color relates to the areas of higher intensity while the highlighted green areas indicate contour lines of equal intensity. Since the desired pattern is transferred into a negative resist, the minima of the intensity pattern have been outlined with green contours to reflect the part of the interferogram that will generate the pattern. Additional minima and maxima are generated adjacent to those in the zero phase shift case. With increasing phase shift the newly created pattern expands and a symmetric twin-like motif is formed at phase shift of  $\pi/2$ , where two elliptical intensity minima are separated by a nanogap. The ratio of the two local intensity minima  $I_1$  and  $I_2$  describes the intensity variation with the change of phase delay, that is, the relative size of the written features in the twin motive. At a phase angle of  $90^\circ$ , variation of the gap size between  $I_1$  and  $I_2$  can be simply achieved by varying the exposure dose, which leads to larger (smaller) holes and thus to smaller (larger) gap size.

While the above-described mechanism for creating nanometer gaps is sufficient for some plasmonic applications, other approaches require motive features with sharp tips, that is, contour shapes similar to what is done with electron beam lithography to create bowtie nanoantennas.<sup>39,40</sup> To this end, we show that changing the polarization state of the second beam can provide a bowtie like shape in the interference pattern. As shown in Figure 3a, the rotation of the linear polarization vector of one beam causes a distortion of the twin motif where both parts diverge and approach their diagonally situated neighbor. At same time, the pattern changes from circular to tiplike shapes forming a bowtielike structure. The achievable separation distance can be calculated from the intensity minima in the contour plots as shown in Figure 3b as a function of rotated polarizer angle  $\theta$ . Clearly, with this technique the two new partners can be approximated until they merge, thereby providing bowtie nanoantennas with gap sizes only limited by the resist resolution.

**Experimental Results.** In order to demonstrate the efficacy of the above technique, we fabricated several twin and triplet motif nanogap arrays arranged in a hexagonal lattice. The hexagonal lattice geometry is particularly well suited for nanoplasmonic applications since it maximizes the number of local hot-spots per unit area as compared to square lattice with the same lattice constant. The exposure was carried out with the 488 nm line of an argon-ion laser. The desired interferometric pattern was achieved by first splitting the initial laser beam into 4 equal intensity arms, introducing half wave plates into each of the arms, and then recombining the beams as shown in Figure 1. Further details of the fabrication procedures are given in the Supporting Information.

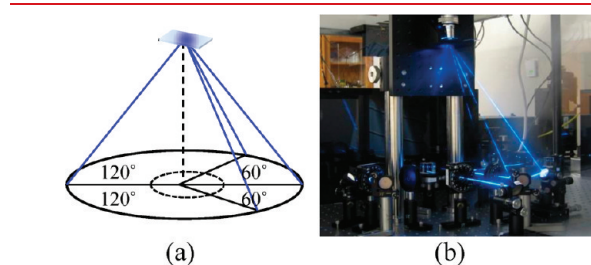


**Figure 1.** (a) Schematic representation of the upside-down umbrella geometry of the four beam HL and (b) photograph of the corresponding experimental setup.

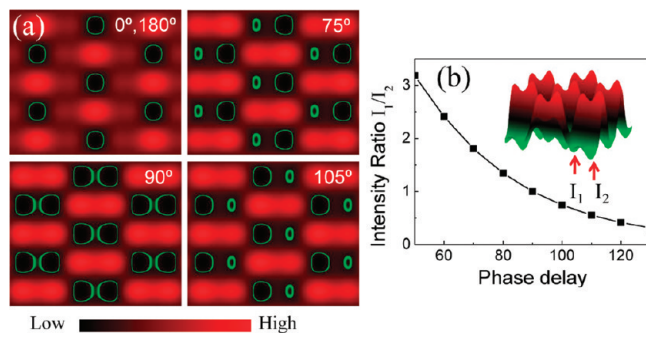


**Figure 2.** (a) Contour plot of the interference profiles for phase angles of 0, 75, 90, 105, and 180°. The green outline highlights the isointensity minima that are used to generate the pattern in the negative resist. (b) Plot of intensity ratio of two highlighted local minima  $I_1$  and  $I_2$  (indicated by arrows) as a function of the phase delay. Inset: 3D plot of the intensity profile at 75°.

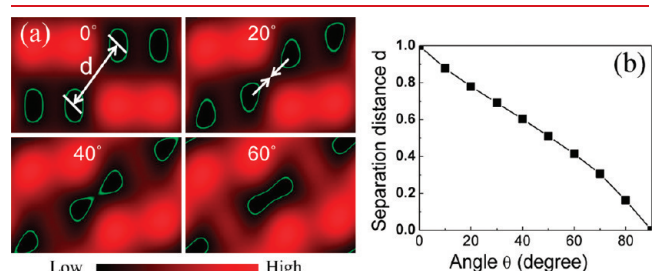


**Figure 3.** (a) Contour plots produced by varying the polarization vector in one of the interferometric arms. The green outline highlights the isointensity minima. (b) Calculated normalized separation distance  $d$  (distance between two local minima) as a function of the varied polarization angle  $\theta$  of one beam.

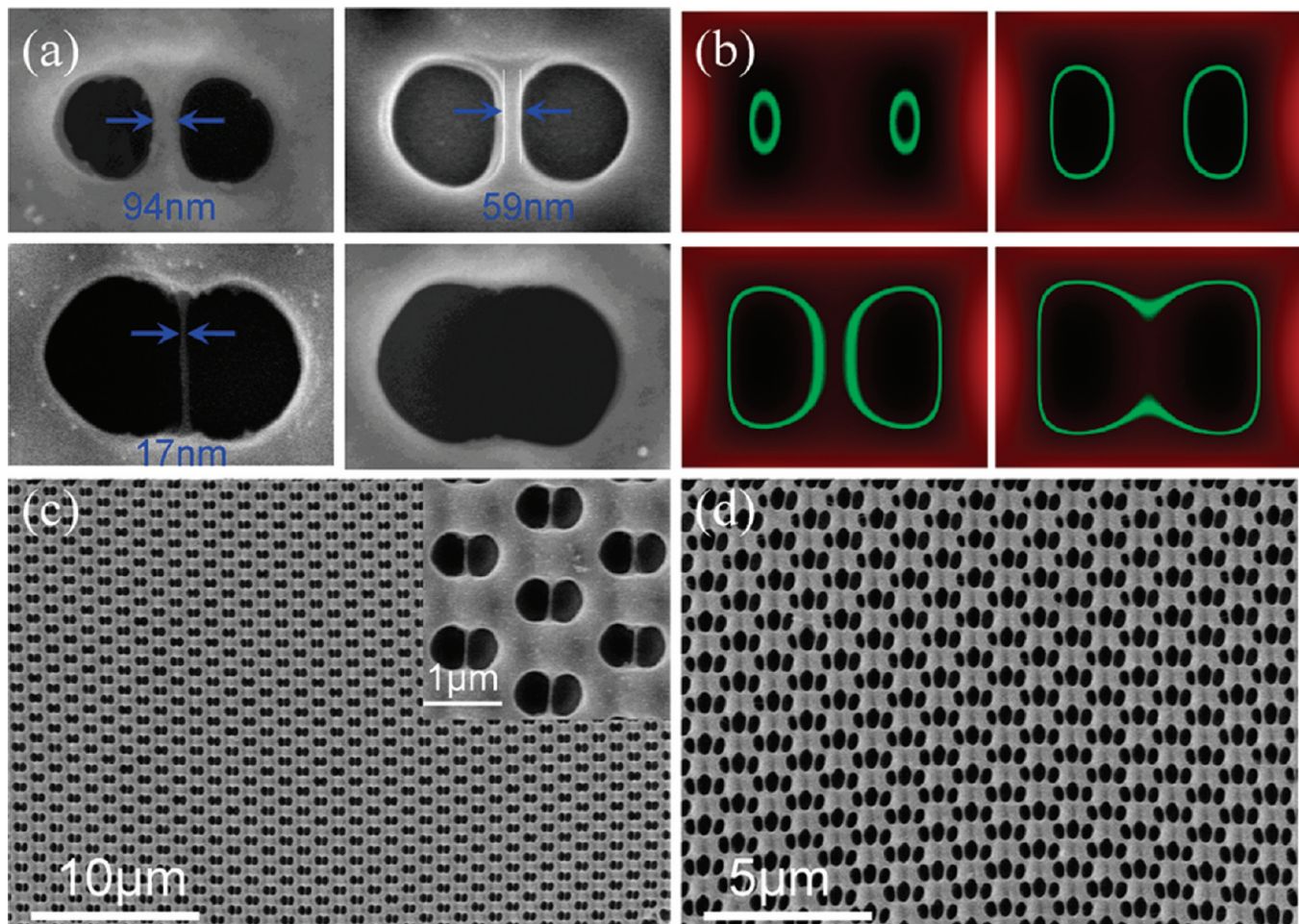


**Figure 4.** (a) SEM images and (b) numerical simulations of the decreasing gap size achieved by increasing the exposure dose. (c) SEM image of a large scale hexagonal nanogap array template, and (insert) a zoom of the hexagonal unit cell. (d) An SEM image of hexagonal triple-hole array.

Note that even a small misalignment of the laser beams can lead to a drastic change in the resultant pattern. If one of the beams is misaligned by more than  $0.2^\circ$ , a periodically varying phase shift is introduced into the exposure area causing striations in the resultant structure, as shown in the Supporting Information. Careful alignment can eliminate these unwanted features in the pattern.

The most facile way to control the size of the resultant nanogap within the framework of holographic nanolithography is achieved by varying the exposure dose at the interference plane. Systematically smaller features are obtained by increasing the exposure dose that results in larger holes and, consequently, smaller gaps. Figure 4a shows four exemplary nanogaps with progressively smaller separations down to 17 nm. The gap sizes realized in these experiments are in good agreement with theoretical predictions, as shown in Figure 4b. Once the exposure dose becomes sufficiently large, the gaps merge forming a diabolo structure. Unlike nanogaps, which concentrate electrical fields within the gap, diabolo nanoantennas have recently been predicted to confine the magnetic field,<sup>41</sup> but have not yet been experimentally realized.

In addition to the small feature sizes, HL offers the possibility of creating large, spatially uniform arrays with a single exposure, as shown in Figure 4c for a  $2500 \mu\text{m}^2$  large nanogap array. The

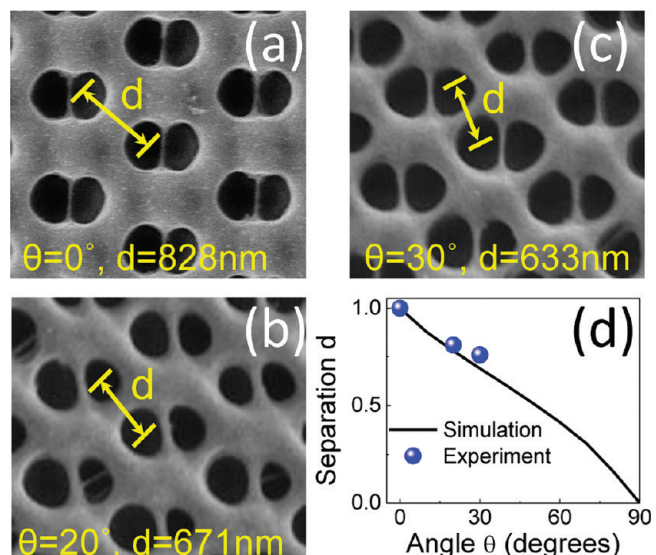


**Figure 5.** Polarization tuning. (a–c) SEM images of the resultant structures produced by rotating a half-wave plate in one of the arms; (d) simulation and experimental results of normalized separation distance  $d$  between two local minima as a function of the orientation of the polarization angle  $\theta$ .

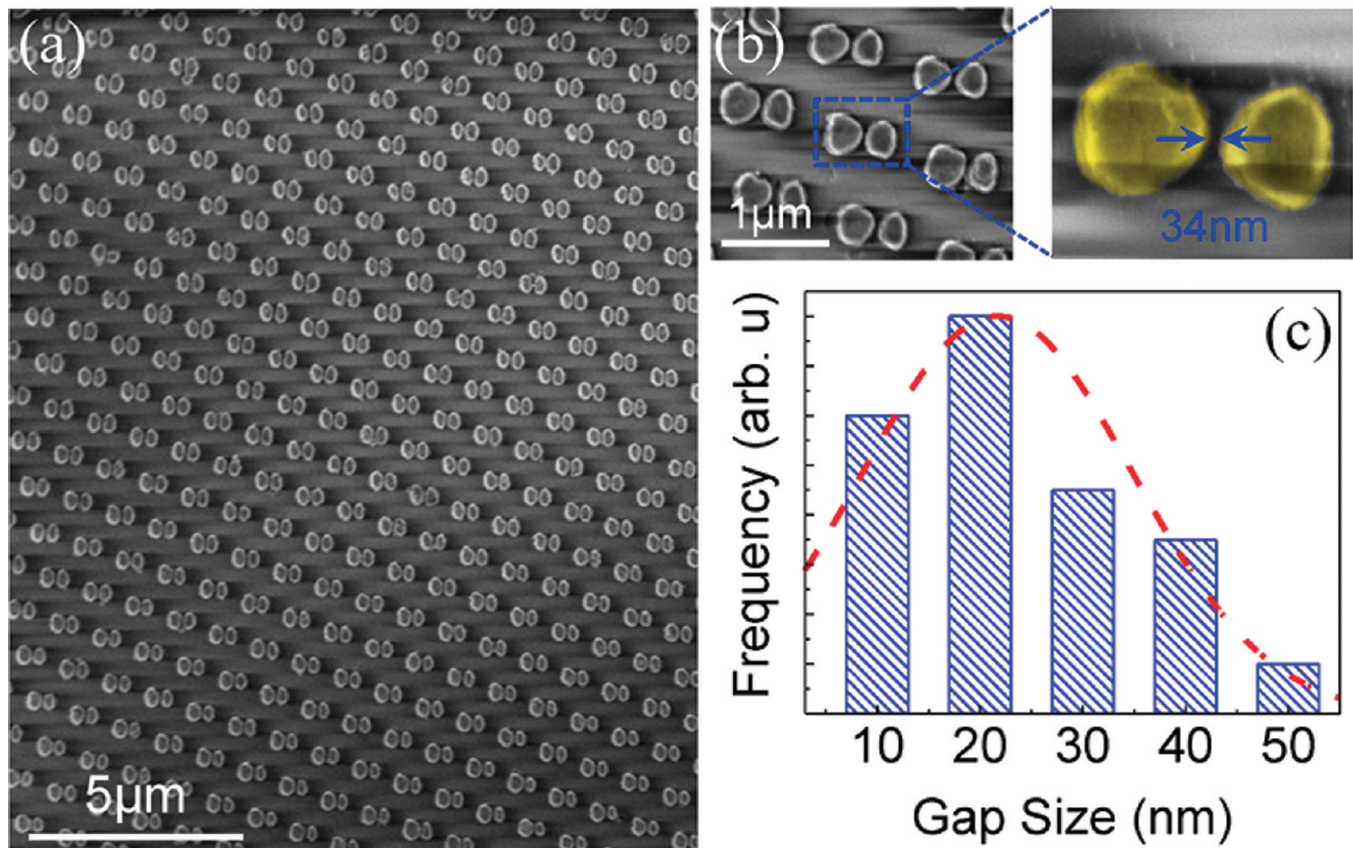


**Figure 6.** (a) An SEM image of a  $500 \mu\text{m}^2$  metallic nanogap array. (b) The bowtie shaped pattern and a magnified image of one structure with a 34 nm gap. (c) Statistical distribution of the gap size taken from 50 nanogaps.

yield of nanogaps is near 100% for feature sizes larger than 50 nm. When the feature size approaches the sub-20 nm region, the residual polymer strands occasionally collapse/break after development and one can estimate that around 10% of the bowtielike structures have no gaps (Figure 4c). The array size in our case was only limited by the laser spot size, and can be enlarged by expanding the laser beam to wafer-scale. The measured lattice constant of 1080 nm for the hexagonal array is in good agreement with a calculated value of 1267 nm when 15% film shrinkage is taken into account.<sup>34,42</sup> In order to further showcase the versatility of the HL technique, we fabricated triplet motive structures as shown in Figure 4d. The triplet motive was realized by changing the polarization of beam 1 from linear to elliptical and introducing a  $150^\circ$  phase delay. Furthermore, a linear polarization angle of  $10^\circ$  in beam 3 and electrical amplitude ratio of  $E/E_2/E_3/E_4 = 2:1:1:2$  were utilized. The resultant triple hole motive is desirable for nanoplasmonic applications since it doubles the number of local hot spots without decreasing the lattice constant, as the latter is fixed by the laser wavelength and is not easily controlled in a typical lithographic process. This triple motive feature has heretofore not been achieved by HL.

In addition to creating triple hole motives, controlling the polarization in each of the interferometric arms can be utilized to decrease the separation  $d$  between pairs of nanogaps while maintaining small hole sizes, as shown in Figure 3. To verify this prediction, we conducted a series of experiments and varied the polarization angle in one of the interferometric arms. As a result, the separation between pairs of nanogaps systematically decreased from 828 to 633 nm and small tiplike holes appear in

the pattern as shown in Figure 5. Note that in contrast to the technique of enlarging the holes using the exposure time to narrow the gap this approach can maintain smaller tiplike holes while decreasing the gap size, as required, for example, for bowtie nanoantennas.

Finally, in order to realize plasmonic structures, several nanopillar arrays were fabricated by filling in the holes in the SU-8 with Cr/Au and removing the residual polymer via a procedure described in the Supporting Information. An SEM of the large array, as well as an exemplary gap, is shown in Figures 6a,b. Following metal evaporation and lift off, statistical analysis of the gap size was carried out, as shown in Figure 6c. The average gap size was found to be 22 nm, and the best gap size obtained was 7 nm. These small gap sizes realized during these experiments are ideal for nanoplasmonic applications such as bowtie nanoantennas, which, for example, were shown to give rise to  $10^6$  SERS enhancement for  $\sim 20$  nm gap sizes.<sup>18,39,43</sup>

The demonstrated HL approach to create large-scale nanoantenna arrays has obvious cost and throughput advantages compared to serial writing tools such as electron beam or AFM lithography. The achieved 90% uniformity over the nanogap array, which can be further optimized, provides advantages when compared to nanosphere lithography, which is limited by a lack of long-range order.<sup>20</sup> Our approach might also offer a novel route to create a periodic master stamp for applications in nanoimprint lithography.

**Summary.** Together, these results demonstrate that 4-beam holographic lithography can be used to create nanogap arrays by tuning the relative position and shape of the twin motive of a compound lattice, which was achieved by utilizing phase,

intensity, and polarization control of the laser beams combined with careful calibration of the resist exposure. Twin and triplet motive features were patterned into an SU-8 mask and transferred into gold to create nanogap arrays with an average gap size of 22 nm and smallest features down to 7 nm, that is, features that are 70 times smaller than the utilized laser wavelength (488 nm). The uniformity and small gap sizes of these arrays make them ideal for nanoplasmonic applications, such as SERS sensing where small gap sizes are essential. Consequently, this work extends the applicability of holographic nanolithography to nanoplasmonic applications.

## ■ ASSOCIATED CONTENT

**S Supporting Information.** Further details of sample preparation, effects of misalignment, metal deposition, and polarization control. This material is available free of charge via the Internet at <http://pubs.acs.org>.

## ■ AUTHOR INFORMATION

### Corresponding Author

\*E-mail strauf@stevens.edu.

## ■ ACKNOWLEDGMENT

We thank Svetlana Sukhishvili and Henry Du for fruitful discussions and the Center for Functional Nanomaterials of the Brookhaven National Laboratory, contract DE-AC02-98CH10886, for the use of their clean rooms. This work was partially supported by the NSF CAREER Program (ECCS - 1053537).

## ■ REFERENCES

- (1) Ozbay, E. *Science* **2006**, *311* (5758), 189–193.
- (2) Anker, J. N.; Hall, W. P.; Lyandres, O.; Shah, N. C.; Zhao, J.; Van Duyne, R. P. *Nat. Mater.* **2008**, *7* (6), 442–453.
- (3) Willets, K. A.; Van Duyne, R. P. *Annu. Rev. Phys. Chem.* **2007**, *58* (1), 267–297.
- (4) Im, H.; Bantz, K. C.; Lindquist, N. C.; Haynes, C. L.; Oh, S. H. *Nano Lett.* **2010**, *10* (6), 2231–2236.
- (5) Kubo, W.; Fujikawa, S. *Nano Lett.* **2011**, *11* (1), 8–15.
- (6) Nam, J.-M.; Thaxton, C. S.; Mirkin, C. A. *Science* **2003**, *301* (5641), 1884–1886.
- (7) Stewart, M. E.; Anderton, C. R.; Thompson, L. B.; Maria, J.; Gray, S. K.; Rogers, J. A.; Nuzzo, R. G. *Chem. Rev.* **2008**, *108* (2), 494–521.
- (8) Bukasov, R.; Shumaker-Parry, J. S. *Nano Lett.* **2007**, *7* (5), 1113–1118.
- (9) Larsson, E. M.; Alegret, J.; Kall, M.; Sutherland, D. S. *Nano Lett.* **2007**, *7* (5), 1256–1263.
- (10) Cao, Y. C.; Jin, R.; Mirkin, C. A. *Science* **2002**, *297* (5586), 1536–1540.
- (11) Min, Q.; Santos, M. J. L.; Girotto, E. M.; Brolo, A. G.; Gordon, R. *J. Phys. Chem. C* **2008**, *112* (39), 15098–15101.
- (12) Novo, C.; Funston, A. M.; Mulvaney, P. *Nat. Nanotechnol.* **2008**, *3* (10), 598–602.
- (13) Narayanan, R.; El-Sayed, M. A. *Nano Lett.* **2004**, *4* (7), 1343–1348.
- (14) Bozhevolnyi, S. I.; Volkov, V. S.; Devaux, E.; Laluet, J.-Y.; Ebbesen, T. W. *Nature* **2006**, *440* (7083), 508–511.
- (15) Lal, S.; Link, S.; Halas, N. J. *Nat. Photonics* **2007**, *1* (11), 641–648.
- (16) Rechberger, W.; Hohenau, A.; Leitner, A.; Krenn, J. R.; Lampecht, B.; Ausseneck, F. R. *Opt. Commun.* **2003**, *220* (1–3), 137–141.
- (17) Fromm, D. P.; Schuck, P. J.; Moerner, W. E.; Sundaramurthy, A.; Crozier, K.; Kino, G. *OSA Trends Opt. Photonics Ser.* **2004**, 725–726.
- (18) Hatab, N. A.; Hsueh, C. H.; Gaddis, A. L.; Retterer, S. T.; Li, J. H.; Eres, G.; Zhang, Z.; Gu, B. *Nano Lett.* **2010**, *10* (12), 4952–4955.
- (19) Mühlischlegel, P.; Eisler, H. J.; Martin, O. J. F.; Hecht, B.; Pohl, D. W. *Science* **2005**, *308* (5728), 1607–1609.
- (20) Xia, D.; Ku, Z.; Lee, S. C.; Brueck, S. R. J. *Adv. Mater.* **2011**, *23* (2), 147–179.
- (21) Raub, A. K.; Li, D.; Frauenglass, A.; Brueck, S. R. J. *J. Vac. Sci. Technol., B* **2007**, *25* (6), 2224–2227.
- (22) Bloomstein, T. M.; Marchant, M. F.; Deneault, S.; Hardy, D. E.; Rothschild, M. *Opt. Express* **2006**, *14* (14), 6434–6443.
- (23) Campbell, M.; Sharp, D. N.; Harrison, M. T.; Denning, R. G.; Turberfield, A. J. *Nature* **2000**, *404* (6773), 53–56.
- (24) Cai, L. Z.; Yang, X. L.; Wang, Y. R. *J. Opt. Soc. Am. A* **2002**, *19* (11), 2238–2244.
- (25) Miklyaei, Y. V.; Meisel, D. C.; Blanco, A.; Von Freymanna, G.; Busch, K.; Koch, W.; Enkrich, C.; Deubel, M.; Wegener, M. *Appl. Phys. Lett.* **2003**, *82* (8), 1284–1286.
- (26) Xu, D.; Chen, K. P.; Ohlinger, K.; Lin, Y. *Appl. Phys. Lett.* **2008**, *93*, 261193.
- (27) Ullal, C. K.; Maldovan, M.; Thomas, E. L.; Chen, G.; Han, Y. J.; Yang, S. *Appl. Phys. Lett.* **2004**, *84* (26), 5434–5436.
- (28) Wang, X.; Ng, C. Y.; Tam, W. Y.; Chan, C. T.; Sheng, P. *Adv. Mater.* **2003**, *15* (18), 1526–1528.
- (29) Wang, X.; Xu, J.; Lee, J. C. W.; Pang, Y. K.; Tam, W. Y.; Chan, C. T.; Sheng, P. *Appl. Phys. Lett.* **2006**, *88* (5), 1–3.
- (30) Pang, Y. K.; Lee, J.; Lee, H.; Tam, W. Y.; Chan, C.; Sheng, P. *Opt. Express* **2005**, *13* (19), 7615–7620.
- (31) Yang, Y.; Li, Q.; Wang, G. P. *Opt. Express* **2008**, *16* (15), 11275–11280.
- (32) Mao, W.; Liang, G.; Zou, H.; Wang, H. *Opt. Lett.* **2006**, *31* (11), 1708–1710.
- (33) Mao, W. D.; Dong, J. W.; Zhong, Y. C.; Liang, G. Q.; Wang, H. Z. *Opt. Express* **2005**, *13* (8), 2994–2999.
- (34) Mao, W.; Liang, G.; Zou, H.; Zhang, R.; Wang, H. Z.; Zeng, Z. *J. Opt. Soc. Am. B* **2006**, *23* (10), 2046–2050.
- (35) Strauf, S.; Hennessy, K.; Rakher, M. T.; Choi, Y. S.; Badolato, A.; Andreani, L. C.; Hu, E. L.; Petroff, P. M.; Bouwmeester, D. *Phys. Rev. Lett.* **2006**, *96* (12), 127404.
- (36) Strauf, S.; Jahnke, F. *Laser Photonics Rev.* **2011**, *5*, DOI: 10.1002/lpor.201000039.
- (37) Begliarbekov, M.; Sul, O.; Santanello, J.; Ai, N.; Zhang, X.; Yang, E.-H.; Strauf, S. *Nano Lett.* **2011**, *11* (3), 1254–1258.
- (38) Han, J.; Craighead, H. G. *Science* **2000**, *288* (5468), 1026–1029.
- (39) Schuck, P. J.; Fromm, D. P.; Sundaramurthy, A.; Kino, G. S.; Moerner, W. E. *Phys. Rev. Lett.* **2005**, *94*, 017402.
- (40) Kinkhabwala, A.; Yu, Z.; Fan, S.; Avlasevich, Y.; Müllen, K.; Moerner, W. E. *Nat. Photonics* **2009**, *3* (11), 654–657.
- (41) Grosjean, T.; Mivelle, M.; Baida, F. I.; Burr, G. W.; Fischer, U. C. *Nano Lett.* **2011**, *11* (3), 1009–1013.
- (42) Wu, L.; Zhong, Y.; Chan, C. T.; Wong, K. S.; Wang, G. P. *Appl. Phys. Lett.* **2005**, *86* (24), 1–3.
- (43) Hao, E.; Schatz, G. C. *J. Chem. Phys.* **2004**, *120* (1), 357–366.